https://doi.org/10.5194/egusphere-2025-6526
Preprint. Discussion started: 5 January 2026


# Along-channel Variability of Total Exchange Flow in a Narrow, Well-mixed Estuary: Influence of the M4 Tide

Manuel Díez-Minguito[1] and Hans Burchard[2]

[1]Andalusian Institute for Earth System Research (IISTA), University of Granada, Avda. del Mediterráneo s/n, Edificio CEAMA, Granada E-18006, Spain

[2]Leibniz Institute for Baltic Sea Research Warnemünde, Physical Oceanography, D-18119 Rostock, Seestr. 15, Germany

**Correspondence:** Manuel Díez-Minguito (mdiezm@ugr.es)

**Abstract.** This study provides preliminary estimates of Total Exchange Flow (TEF) along the Guadalquivir River Estuary (Spain) at notable cross-sections during low river flows. The analysis combines observations recorded during 3 years by a real time monitoring network and analytical model output for a well-mixed $\mathrm{M2}+\mathrm{M4}$ tidal flow with oscillating salinity. Exchange profiles and volume and salinity transports sorted by salinity classes are computed. The results indicate that bulk along-channel TEF estimates decrease upstream.

The largest net incoming water volume transport, viz. approx. $300\,\mathrm{m^3 s^{-1}}$, is attained at the lower part of the estuary, near where the largest salinity gradient is observed. This value is about 12-fold the normal river flow from the head dam at Alcalá del Río. Knudsen-consistent bulk quantities evidence the weakly-stratified character of the Guadalquivir estuary, whose mixing completeness is larger than 67% at all cross-sections. The covariance between salinity and current seems to play a more important role in exchange flow in the Guadalquivir estuary than the effects due to tidal asymmetry.

Overall, the inclusion of the M4 improves TEF estimates in $\sim 10\%$ in the Guadalquivir estuary. A sensitivity analysis shows that in other estuaries and semi-enclosed basins the effects of the M4 could be even larger. The inclusion of the M4 constituent changes thickness and magnitude of the bi-layer exchange flow by salinity class. A remarkable inflow could be obtained at low salinity classes when the estuary exhibits large M4 current amplitude and M4 current phases close to $160^\circ$.

## 1 Introduction

The Total Exchange Flow (TEF) analysis framework represents a paradigm that allows computing the exchange flow in estuaries using isohaline coordinates. Tidally-averaged net volume and mass transport through an estuarine cross-section are obtained sorted by salinity classes (transports as a function of salinity class) (MacCready, 2011; Burchard et al., 2019).

Among its outstanding features are: TEF estimates include transports due to covariance of current velocity and salinity, thereby being consistent with (steady-state) Knudsen-bulk values (Knudsen, 1900; Burchard et al., 2018a) and generalizing

https://doi.org/10.5194/egusphere-2025-6526
Preprint. Discussion started: 5 January 2026


the classical Knudsen relations based on mass and salt conservation; and TEF naturally allows quantifying volume-integrated mixing, which in turn controls the inflow and outflow transport of water and salinity.

Burchard et al. (2019) proposed a simple analytical sectionally-homogeneous tidal model to show that even under tidally-energetic conditions an exchange flow may develop. The model required prescribing M2 tidal amplitudes and phases in such a way that a specified runoff was obtained and that the residual salt transport is zero. These authors obtained TEF Knudsen-bulk estimates for inflow and outflow of water and salt concentrations. Lorenz et al. (2019) provided an algorithm which extends the formulation of the dividing salinity method (MacCready et al., 2018). The algorithm allows to overcome numerical issues regarding the practical computation of TEF for a large number of salinity classes, thereby ensuing convergence to the TEF bulk values. These authors used the same simple analytical tidal model to test the extended dividing salinity method and its convergence. The goodness of the convergence behavior allows extending the method to exchange flows with more than two layers (see, e.g., Burchard et al., 2025).

In this manuscript, the well-mixed M2 tidal flow with oscillating salinity model devised by Burchard et al. (2019) is extended to include the contribution of the M4 tidal constituent, thereby requiring the prescription of both M2 and M4 amplitudes and phases both in current and salinity. The M4 overtide is known to create ebb-flood asymmetry in levels and currents (e.g. Speer and Aubrey, 1985; Parker, 1991; Friedrichs and Aubrey, 1994) and affects the transport of particulate matter (e.g. de Swart and Zimmerman, 2009; Burchard et al., 2018b). The extended model is applied to the Guadalquivir estuary to estimate TEF at various cross-sections, including the mouth. A sensitivity analysis of TEF to the inclusion of the M4 to the tidal flow and salinity model is carried out as well.

To address the estimates of TEF in the Guadalquivir estuary, high-resolution field data of along-channel currents and salinity at seven notable cross-sections was the basis for the analysis. Observations were automatically recorded between 2008 and 2011 by a real time monitoring network (Navarro et al., 2011). The Guadalquivir estuary is a flood-dominated, tidally-energetic estuary that features a well-mixed to partially mixed (near the mouth) water column during low river flow conditions (Díez-Minguito et al., 2012, 2013). The analysis combines those observations and the analytical model for a well-mixed $\mathrm{M2}+\mathrm{M4}$ tidal flow model with oscillating salinity. Exchange profiles and volume and salinity transports sorted by salinity classes were computed. To address the sensitivity analysis of the TEF to the overtide M4, a set of simulations was performed including a M4 term to the tidal flow and salinity model. The ratio between M4 and M2 current and salinity amplitudes, as well as the difference between M4 current and salinity phases, is varied. Effects in exchange profiles, and thus in volume transports, salinities, and salt transports, are examined.

The study is organized as follows. Section 2 sets the TEF framework and introduces the oscillating and well-mixed $\mathrm{M2}+\mathrm{M4}$ tidal flow model (subsection 2), and describes the Guadalquivir estuary study area (subsection 2.3) and the field measurements recorded in it (subsection 2.4). The TEF estimates are described in the Results and Discussion Section 3. The results, along with the sensitivity analysis of the TEF to the overtide M4, and their implications are discussed in the same Section. Main conclusions are drawn in Section 4.

https://doi.org/10.5194/egusphere-2025-6526
Preprint. Discussion started: 5 January 2026


## 2 Formulation and Methodology

### 2.1 TEF Framework

According to the TEF analysis framework, the time-averaged volume transport per salinity class $Q$ through a given cross-section $A$ with salinity $s$ greater than a given value $S$ is obtained as

$$Q(S) = \overline{\int_{A(s\geq S)} u \,\mathrm{d}A}\,, \tag{1}$$

where the bar $\bar{\cdot}$ indicates time-averaging, and $u$ is the along-channel current normal to the cross-section $A$. Changes in cross-sectional area due to tides are not taken into account.

From Eq. 1 the exchange profile of water transport per salinity class is obtained as

$$q(S) = \frac{\mathrm{d}Q(S)}{\mathrm{d}S}\,, \tag{2}$$

which verifies $Q = \int_{s\geq S} q(s)\, ds$. Separating incoming and outgoing volume transports, it reads

$$Q_{in} = \int_{S_{min}}^{S_0} q \,\mathrm{d}s\,, \qquad Q_{out} = \int_{S_0}^{S_{max}} q \,\mathrm{d}s\,, \tag{3}$$

where $S_0$ is the dividing salinity which separates the inflow and outflow, and $S_{min}$ and $S_{max}$ are the minimum and maximum salinities in the cross-section. Equation 3 assumes the incoming and outgoing flows arrange in two layers, as the classical estuarine circulation. Lorenz et al. (2019) also generalized the formulation for exchange flows with more than two layers.

Similarly to Eqs. 1 and 2, the time-averaged transport of salt, $Q^s$, reads

$$Q^s(S) = \overline{\int_{A(s\geq S)} s\,u \,\mathrm{d}A}\,, \tag{4}$$

where $Q^s = \int_{s\geq S} q^s(s)\,\mathrm{d}s$ and

$$Q^s_{in} = \int_{S_{min}}^{S_0} q^s \,\mathrm{d}s\,, \qquad Q^s_{out} = \int_{S_0}^{S_{max}} q^s \,\mathrm{d}s\,. \tag{5}$$

Based on quantities defined in Eqs. 3 and 5, Kundsen-consistent salt concentration for in- and outflows at a cross-section are

$$s_{in} = \frac{Q^s_{in}}{Q_{in}}\,, \qquad s_{out} = \frac{Q^s_{out}}{Q_{out}}\,. \tag{6}$$

From Eq. 6, the volume-integrated mixing (understood as destruction of volume-integrated salinity variance), which is related to the exchange flow, is $M \approx s_{in} s_{out} Q_r$, where $Q_r$ is the river flow. Considering the maximum possible mixing $M_{\max} = s_{in}^2 Q_r$, the mixing completeness is defined as (MacCready et al., 2018; Burchard et al., 2019)

$$MC = M/M_{\max} = s_{out}/s_{in}\,. \tag{7}$$

https://doi.org/10.5194/egusphere-2025-6526
Preprint. Discussion started: 5 January 2026


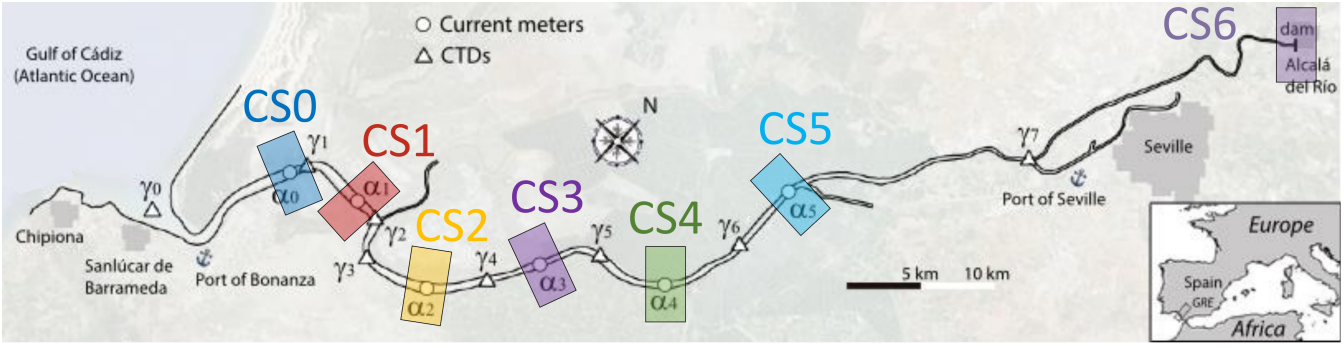


**Figure 1.** Map of study area. Data in this work is obtained from current-meter profilers, ADCPs (circles, $\alpha_i$), and environmental quality probes or CTDs (triangles, $\gamma_i$). Cross-sections $\mathrm{CS_i}$ (Fig. 1), with $i = 0, \ldots, 5$ are defined by the location of the current meters $\alpha_i$. Salinity tidal data are linearly interpolated at $\alpha_i$ locations.

### 2.2 Oscillating and Well-Mixed Tidal Flow

Tidal current and salinity are assumed a superposition of the main semidiurnal constituent M2 and their most energetic overtide M4 as

$$u(x,t) = u_r(x) + u_a(x)\cos(\omega_{\mathrm{M2}}t) + u_b(x)\cos(\omega_{\mathrm{M4}}t + \varphi_b(x)) \tag{8a}$$

$$s(x,t) = s_r(x) + s_a(x)\cos(\omega_{\mathrm{M2}}t + \psi_a(x)) + s_b(x)\cos(\omega_{\mathrm{M4}}t + \psi_b(x)) \tag{8b}$$

with $x$ indicating the along-channel location of the cross-section, $u_r$ the residual current induced by the river flow, $s_r$ the mean salinity, $u_a$ and $u_b$ the current M2 and M4 amplitudes, $\varphi_b$ the current M4 phase relative to that of the M2, $s_a$ and $s_b$ the salinity M2 and M4 amplitudes, and $\psi_a$ and $\psi_b$ the salinity M2 and M4 tidal phases relative to the current M2 phase. Residuals, amplitudes and phases are obtained (and prescribed) from field measurements (described below). Tidal periods are $T_{\mathrm{M2}} = 2\pi/\omega_{\mathrm{M4}} = 12.42\,\mathrm{hr}$ and $T_{\mathrm{M4}} = 2\pi/\omega_{\mathrm{M4}} = 6.21\,\mathrm{hr}$.

The tidally-averaged (residual) salinity flux $\overline{u \cdot s}$ through a given cross-section at $x$ is obtained from Eq. 8a and 8b as

$$\overline{u \cdot s} = u_r s_r + \frac{u_a s_a}{2}\cos(\psi_a) + \frac{u_b s_b}{2}\cos(\varphi_b - \psi_b)\,. \tag{9}$$

Zero residual salinity flux, i.e. $\overline{u \cdot s} = 0$, implies

$$\cos(\psi_a) = -2\frac{u_r s_r}{u_a s_a} - \frac{u_b s_b}{u_a s_a}\cos(\varphi_b - \psi_b)\,. \tag{10}$$

This zero flux condition reduces the degrees of freedom of the problem to eight, to be determined from observations: $u_r$, $s_r$, $u_a$, $s_a$, $u_b$, $s_b$, $\varphi_b$ and $\psi_b$. Considering the M2 tide only in Eqs. 8a and 8b, as in Burchard et al. (2019); Lorenz et al. (2019), the condition of zero residual salinity transport would reduce to $\cos(\psi_a) = -2(u_r s_r)/(u_a s_a)$.

https://doi.org/10.5194/egusphere-2025-6526
Preprint. Discussion started: 5 January 2026


### 2.3 Study Area

The Guadalquivir River Estuary is a coastal-plain estuary located in the south-western part of the Iberian Peninsula. The Guadalquivir estuary comprises the last $110\,\mathrm{km}$ of the Guadalquivir river, from head dam at the town of Alcalá del Río to Sanlúcar de Barrameda, where its waters flow into the Gulf of Cádiz in the Atlantic Ocean (Fig. 1). The estuary is convergent with tidally-averaged cross-sections approximately decreasing exponentially from the mouth to the landward end according to

$$A(x) = A_0 \exp\left(-x/a_0\right), \tag{11}$$

with $A_0 = 5839.4\,\mathrm{m}^2$ and $a_0 = 60.26\,\mathrm{km}$. Its mean depth in the *thalweg*, $h \approx 7\,\mathrm{m}$, is maintained by periodic dredging of the navigation channel (Sirviente et al., 2023). Tides are mesotidal (vertical tidal range at spring tides $\sim 3.5\,\mathrm{m}$ at the mouth) and semidiurnal, being the M2 is the most significant constituent. Tidal amplitudes for the M2, S2, K1, and M4 constituents at the mouth are, respectively, $92.4_{0.2}\,\mathrm{cm}$, $32.60_{0.20}\,\mathrm{cm}$, $6.51_{0.10}\,\mathrm{cm}$, and $3.81_{0.01}\,\mathrm{cm}$ (Díez-Minguito et al., 2012). The estuary is flood-dominated as evidenced by the tidal phase differences between M2 and its first overtide M4, which accounts for (intra)tidal asymmetry. The wave propagation is dominated by friction and in the upper part by tidal wave reflection at the head dam of Alcalá del Río dam (Díez-Minguito et al., 2012; Muñoz-Lopez et al., 2024).

The climate in most of the Guadalquivir watershed is Mediterranean. The discharge regime is highly conditioned by the extensive upstream regulation of the catchment. Freshwater discharges from the Alcalá del Río dam are usually below $Q_r = 40\,\mathrm{m}^3\mathrm{s}^{-1}$, most often about $Q_r \sim 25\,\mathrm{m}^3\mathrm{s}^{-1}$. Salinity decreases from the mouth upstream due to freshwater input. The mesotidal conditions along with the relatively low values of $Q_r$ make the estuary tidally-energetic and well-mixed (partially-mixed near the mouth) in terms of salinity during low river flows. This is confirmed by the low values of the estuarine Richardson number ($Ri_E < 0.08$) and the potential energy anomaly (Cobos et al., 2020). Díez-Minguito et al. (2013) determined from an observational analysis that time correlation between tidal flow and salinity controls a substantial part of the salt transport. Modeling results by Biemond et al. (2024) showed that the salt transport due to the exchange flow interacts with that of the current-salinity correlation and that both transports are equally important in the Guadalquivir estuary. Under low river flow conditions, most of the observed suspended matter in the Guadalquivir estuary is due to the resuspension by tidal currents (Díez-Minguito et al., 2014; Díez-Minguito and de Swart, 2020). The transport due to the M2 and M4 covariance of current velocity and suspended sediment explains the setting of Estuarine Turbidity Maxima in the Guadalquivir estuary (Caballero et al., 2014; Díez-Minguito et al., 2014).

### 2.4 Data Collection

Salinity and current data were recorded between 2008 and 2011 by a real time monitoring network, which was described in detail by Navarro et al. (2011) and depicted in Fig. 1. Here only a brief description of the equipment is provided. Instrumentation was installed as close as possible to the navigation channel. Salinity data was recorded every 30 minutes in eight Conductivity-Temperature-Depth (CTD, denoted by $\gamma_i$ in Fig. 1) probes. The origin of the along-channel coordinate $x$ was set at $\gamma_0$, installed at the mouth of the estuary, and chosen chosen positive upstream. Table 1 shows the locations of the CTDs used in this study.

https://doi.org/10.5194/egusphere-2025-6526
Preprint. Discussion started: 5 January 2026


Along-channel current data was obtained from six Acoustic Doppler Current Profilers (ADCPs) ($\alpha_i$ in Fig. 1). They provided one data set every 15 min. Table 1 shows the kilometer points and geographic coordinates where the ADCPs were located in the Guadalquivir estuary.

**Table 1.** Locations where the CTDs ($\gamma_i$) and ADCPs ($\alpha_i$) were located, with respect to the estuary mouth, and tidally-averaged cross-sections computed using Eq. 11 at the ADCP locations.

| CTD | $\gamma_1$ | $\gamma_2$ | $\gamma_3$ | $\gamma_4$ | $\gamma_5$ | $\gamma_6$ |
|---|---|---|---|---|---|---|
| [km] | 17.30 | 23.60 | 26.20 | 35.30 | 47.10 | 57.60 |
| ADCP | $\alpha_0$ | $\alpha_1$ | $\alpha_2$ | $\alpha_3$ | $\alpha_4$ | $\alpha_5$ |
| [km] | 14.30 | 20.80 | 31.80 | 39.80 | 49.30 | 63.80 |
| $A$ | $\alpha_0$ | $\alpha_1$ | $\alpha_2$ | $\alpha_3$ | $\alpha_4$ | $\alpha_5$ |
| [$m^2$] | 4606 | 4135 | 3445 | 3017 | 2577 | 2026 |

**Table 2.** Harmonic analysis of the along-channel horizontal tide time series. Amplitudes are in $\mathrm{cm\,s^{-1}}$ and phases in ° Greenwich. Errors (subscripts) corresponds to the 95% confidence interval. Subtracting the current M2 phase to the current M4 phase, $\varphi_b$ is obtained as the M4 phase relative to that of the M2, as defined in Eqs. 8a and 8b.

| - | Amp. M2 $u_a$ [$\mathrm{cm\,s^{-1}}$] | Phase M2 [°] | Amp. M4 $u_b$ [$\mathrm{cm\,s^{-1}}$] | Phase M4 [°] |
|---|---|---|---|---|
| $\alpha_0$ | $63_7$ | $54_5$ | $5_2$ | $100_{30}$ |
| $\alpha_1$ | $100_5$ | $63_3$ | $3.9_{1.3}$ | $100_{20}$ |
| $\alpha_2$ | $50_6$ | $69_9$ | $2_3$ | $150_{60}$ |
| $\alpha_3$ | $69_4$ | $77_3$ | $5.1_{1.2}$ | $250_{12}$ |
| $\alpha_4$ | $72_3$ | $85_3$ | $4.0_{2.3}$ | $250_{30}$ |
| $\alpha_5$ | $55_3$ | $90_3$ | $8.5_{2.0}$ | $196_{13}$ |

**Table 3.** Harmonic analysis of the salinity time series. Residual values and amplitudes are in psu and phases in ° Greenwich. Errors (subscripts) corresponds to the 95% confidence interval. Subtracting the current M2 phase to the salinity M2 and M4 phases, $\psi_a$ and $\psi_b$ are obtained as the salinity M2 and M4 tidal phases relative to the current M2 phase, respectively, as defined in Eqs. 8a and 8b.

| - | Amp. M2 $s_a$ [psu] | Phase M2 [°] | Amp. M4 $s_b$ [psu] | Phase M4 [°] | Residual $s_r$ [psu] |
|---|---|---|---|---|---|
| $\gamma_1$ | $5.50_{0.15}$ | $137.9_{1.4}$ | $0.61_{0.04}$ | $214_5$ | 22.5 |
| $\gamma_2$ | $4.10_{0.15}$ | $139.7_{2.4}$ | $0.37_{0.06}$ | $171_9$ | 17.5 |
| $\gamma_3$ | $3.81_{0.11}$ | $146.0_{1.8}$ | $0.29_{0.05}$ | $226_{11}$ | 15.5 |
| $\gamma_4$ | $2.36_{0.07}$ | $153.3_{1.7}$ | $0.16_{0.03}$ | $265_{11}$ | 10.0 |
| $\gamma_5$ | $1.29_{0.03}$ | $158.3_{1.5}$ | $0.06_{0.01}$ | $201_{15}$ | 7.0 |
| $\gamma_6$ | $0.79_{0.04}$ | $161.3_3$ | $0.10_{0.01}$ | $284_5$ | 4.0 |

Standard harmonic analysis was performed on the along-channel current and salinity time series using T_TIDE (Pawlowicz et al., 2002). Results are shown in Tables 2 and 3. The time span for the harmonic analysis was June 5, 2008 through December 5, 2008. This time span was chosen according to the following three criteria. The interval must be larger than 28 days to separate the M2 from other semidiurnal constituents and to assure a zero residual net salt flux. And, finally, the chosen interval is that

https://doi.org/10.5194/egusphere-2025-6526
Preprint. Discussion started: 5 January 2026


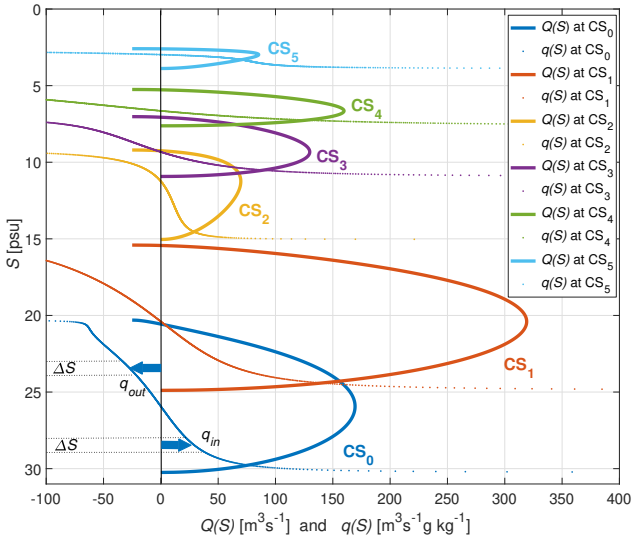


**Figure 2.** Volume transports $Q(S)$ (solid curves) and exchange profiles (dotted curves) $q(S)$ sorted by salinity classes are computed at cross-sections $\mathrm{CS}_i$. Notice the inversion of the vertical axis.

one with the fewer and smaller exceedances over $40\,\mathrm{m^3 s^{-1}}$ to assure that the data analysis corresponds with low river flow conditions.

Daily discharge data records at Alcalá del Río were provided by the Regional Water Management Agency (Red de seguimiento de la Confederación Hidrográfica del Guadalquivir, MAPAMA, station code 5072).

## 3 Results and Discussion

### 3.1 Volume Transports, Exchange Profiles and Bulk Quantities

Volume transports and exchange profiles sorted by salinity classes are computed numerically using the analytical time series from Eqs. 1 and 2, respectively. They are computed at different cross-sections along the Guadalquivir estuary indicated in Table 1 (and Fig. 1). Tidal currents and salinity are obtained from the oscillating and well-mixed tidal flow model Eqs. 8a and 8b, which include both the M2 and M4 constituents.

Values of $u_r$, $s_r$, $u_a$, $s_a$, $u_b$, $s_b$, $\varphi_b$ and $\psi_b$ (Eqs. 1 and 2) at each cross-section in Fig. 1 are thus needed. They are obtained from Table 2 and 3. From Eq. 10, $\psi_a$ is also computed from the other eight parameters at each cross-section. Differences between observed values of $\psi_b$ (Table 3) and those determined from Eq. 10 imposing zero residual salt flux are smaller than $12°$ at all cross-sections, i.e., $\{5.45°, 11.20°, 1.70°, 5.54°, 7.80°, 2.16°\}$. Therefore, at the analysis scale, the estuary can be reasonably considered close to equilibrium conditions (zero residual salt flux).

Figure 2 shows the isohaline volume transport (solid lines) and the exchange profile (dotted lines), which are computed numerically using analytical time series according to Eqs. 1 and 2, respectively, as a function of the salinity at cross-sections

https://doi.org/10.5194/egusphere-2025-6526
Preprint. Discussion started: 5 January 2026


$CS_i$. Overall, as the tide propagates upstream, i.e., towards estuarine parts of lower salinity and current, the maximum values of $Q(S)$ become smaller. The largest volume transports $Q(S)$ are observed at the $CS_1$ and $CS_0$ cross-sections, which are in the lower part of the estuary where the tidal currents are larger. The exchange profile $q(S)$ is structured in two layers at all locations, thereby showing a incoming transport of water per salinity class ($q_{in}$) at higher salinity and an outgoing transport at lower salinity ($q_{out}$). It is evident from Fig. 2 that incoming and outgoing transport vary more by salinity class in locations near the estuary mouth.

Figure 3 shows the Knudsen-consistent bulk along-channel TEF values, $Q_{in}$ and $Q_{out}$, determined integrating $q_{in}$ and $q_{out}$ (Eq. 3), i.e. positive and negative transports, respectively. The results indicate that bulk along-channel exchange flow tends to decrease upstream, as expected. Incoming and outgoing water volume transports are about 10% larger than previous estimates based on gravitational circulation only (Reyes-Merlo et al., 2013). At the landward boundary at the head dam ($CS_6$), the outgoing volume transport coincides with the freshwater discharge $Q_r = -25\,\mathrm{m^3 s^{-1}}$. Negligible values are obtained in the upper part of the estuary near the head dam. In the middle part of the estuary, incoming TEF bulk volume values below $150\,\mathrm{m^3 s^{-1}}$ are obtained. The largest net incoming water volume transport, viz. $Q_{in} \approx 300\,\mathrm{m^3 s^{-1}}$, is attained at the lower part of the estuary at $CS_1$. The outgoing bulk value at $CS_1$ is about 12-fold the normal river flow from the head dam at Alcalá del Río.

It is evident from the TEF results shown in Fig. 3 that the exchange flow does not decrease continuously from the estuary mouth to the head. The along-channel variability of the bulk estimates (from Eq. 5) are mainly due to changes in the along-channel currents and distribution of salinity. Cross-section $CS_1$ is the closest to where the largest (averaged) along-channel salinity gradient (Díez-Minguito et al., 2013) and where the largest tidal currents are observed (Table 2). The relative exchange flow mininum at cross-section $CS_2$ is caused by a significant decrease of the M2 tidal current amplitude (Table 2). A plausible source of variability could be due lateral variations in the along-channel current over the cross-section. Although instrumentation was installed as close as possible to the main channel of the estuary, the particular mooring location of each current meter may also affect tidal current amplitudes and, thus, TEF estimates. The exchange flow minimum at cross-section $CS_2$ suggests that further upstream outflows are convergent and inflows are divergent, which can only be explained by a partial recirculation of the outflow towards the estuary head. Directly downstream of the minimum, outflow is divergent and inflow is convergent such that parts of the inflow is deflected back towards the mouth of the estuary. This mechanism has been described by Cokelet and Stewart (1985) as the efflux/reflux theory. In practice, this would imply larger residence times for conservative pollutants.

It should be noted that exchange flow in a well-mixed estuary does not mean that there is a distinct upstream flow of salty water near the bottom and a downstream flow of brackish water near the surface, even though the exchange profiles $q(S)$ are structured in two layers (as in Fig. 2). The exchange flow following the Knudsen (1900) theory is formulated in salinity coordinates and means that the outflow $Q_{out}$ occurs at lower salinities than the inflow $Q_{in}$. During flood a water parcel with a specific salinity passes through a transect, leaving an upstream flux contribution at a certain salinity class. Upstream of the transect, this water parcel exchanges salinity with other water parcels, such that during ebb it passes the transect at a different salinity, leaving a downstream contribution at this different salinity. Statistically, the flood flux happens at a higher salinity than the ebb flux, due to the lower salinities upstream, caused by the freshwater discharge from the river. This is why the fully

https://doi.org/10.5194/egusphere-2025-6526
Preprint. Discussion started: 5 January 2026


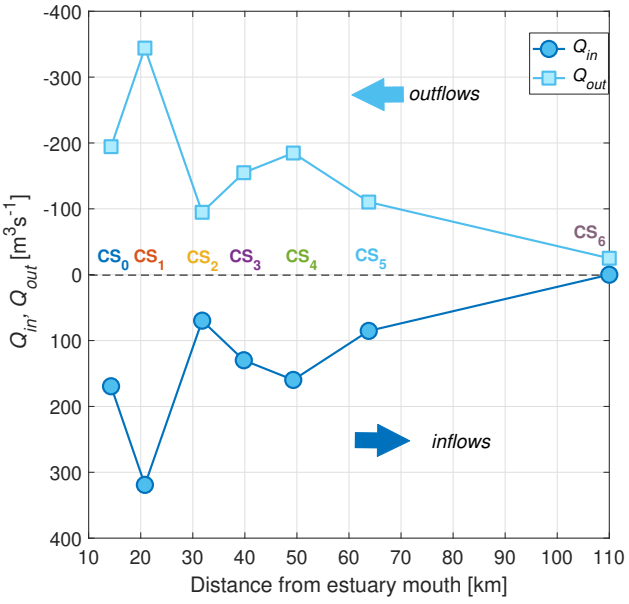


**Figure 3.** Outgoing $Q_{out}$ (light blue curve, squares) and incoming $Q_{in}$ (dark blue curve, circles) volume transports at each cross-section $\mathrm{CS}_i$.

cross-sectionally mixed idealised estuarine situation described in eqs. (8a) and (8b) still results in an estuarine exchange flow, when formulated in salinity coordinates.

Figure 4 shows the along-channel Knudsen consistent salt concentrations within inflows and outflows at each cross-section. Both curves resemble the (averaged) salinity along-channel distribution of salinity. The representative TEF bulk salinity values for the incoming transport are larger than those for the outgoing transport. Differences increase towards the estuary mouth from the head dam, where $s_{in} = s_{out} = 0$. At $\mathrm{CS}_0$, which is the cross-section nearest to the mouth, the representative TEF bulk salinity value for inflows is $28\,\mathrm{psu}$, whereas that for outflows at the same location is about $21\,\mathrm{psu}$. Where the largest net incoming water volume transport occurs ($\mathrm{CS}_1$) these values are $16\,\mathrm{psu}$ and $24\,\mathrm{psu}$, respectively.

### 3.2 Mixing Completeness

The small differences between representative TEF bulk salinity values for outflows and inflows ensue from the high rates of mixing in the Guadalquivir estuary. According to Burchard (2020), the volume-integrated mixing can thus be approximated by $M \approx s_{in} s_{out} Q_r \approx s^2 Q_r$, assuming here that $s = (s_{in} + s_{out})/2$. The local mixing per salinity class is estimated as $\partial M / \partial s \approx 2 Q_r s$, which varies linearly with salinity. This gives a gross estimate of the discharge through the isohaline (related with the entrainment velocity through isohalines) of $\sim Q_r$. This results is postulated as an universal relation of estuarine mixing (Burchard, 2020). The analysis of salt transport indicates that the mixing completeness, estimated from Eq. 7 (in %), is larger than 67% at all cross-sections (Fig. 5), thereby evidencing the poorly-stratified character of the Guadalquivir estuary. The

https://doi.org/10.5194/egusphere-2025-6526
Preprint. Discussion started: 5 January 2026


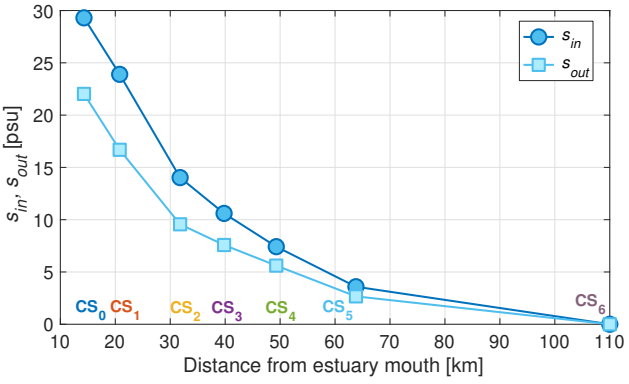


**Figure 4.** Knudsen consistent salinities for in- (dark blue curve, circles) and outflows (light blue curve, squares) at cross-sections along the estuary.

mixing completeness attains $\sim 72\%$, which corresponds to an integrated mixing of $\sim 1.6 \cdot 10^4\,\mathrm{m^3 s^{-1} g^2 kg^{-2}}$, at the cross-section nearest to the mouth of the estuary. The net TEF exchange of variance upstream, at the tidal river part, is negligible and the mixing is complete.

Mixing completeness values in the lower and middle part of the Guadalquivir estuary, which are between $70\%$ and $75\%$, are similar to the $75\%$ estimated near the mouth of the Elbe during high discharge conditions (Reese et al., 2024). The estimated values in the Guadalquivir are not far from those obtained in and idealized convergent V-shaped model estuary, viz. $64\%$ (MacCready et al., 2018), which seems reasonable as the Guadalquivir estuary is a highly channelized estuary. As the mixing is complete at the head dam, and also according to the increasing upstream trend shown in Fig. 5, the upper part of the Guadalquivir estuary is expected to exhibit high mixing completeness values. A reference value in that sense could be the $87\%$ estimated in the Hudson river estuary at The Battery during spring tides (Wang et al., 2017). Nevertheless, estimated values in the Guadalquivir estuary have to be considered as time-averaged and modulation of the mixing completeness by (e.g.) the spring-neap cycle are expected. Overall, mixing estimates from $M$ have shown errors of at most $10\%$ from the real mixing, according to Burchard et al. (2019). Better estimates of mixing could be attained considering time-dependent inflows and outflows as well as storage terms for volume, salt, and salt squared.

### 3.3 Influence of M4 in Total Exchange Flow

#### 3.3.1 Guadalquivir Estuary

The inclusion of the M4 tidal constituent in the analysis, with regards to the original analysis of the M2(-only) tidal flow model by Burchard et al. (2019); Lorenz et al. (2019), produces noticeable effects in both the volume transports $Q(S)$ and exchange profiles $q(S)$. Figure 6 shows results of $Q$ and $q$ per salinity class at cross-sections $\mathrm{CS}_i$ for the extended tidal model, which includes the M4 and M2 contribution (colored curves), and that with the M2 constituent only (black curves). Colored curves are in fact the same as in Fig. 2. Differences in magnitude between both are evident at all cross-sections, but they are somehow

https://doi.org/10.5194/egusphere-2025-6526
Preprint. Discussion started: 5 January 2026


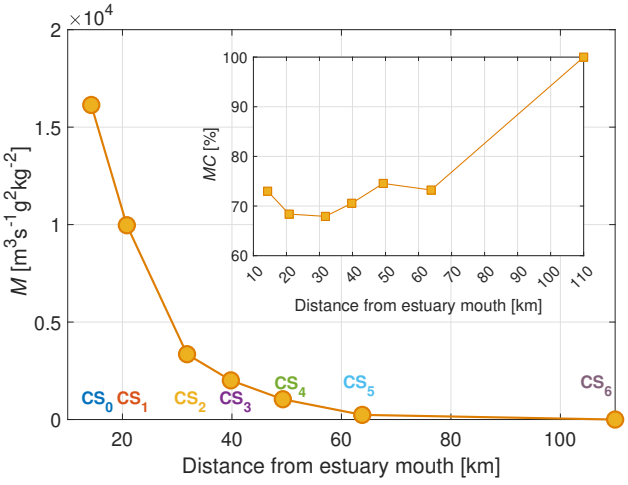


**Figure 5.** Volume-integrated mixing and mixing completeness (inset).

more acute at $\mathrm{CS}_0$ and $\mathrm{CS}_5$. The M4 inclusion does not change the two-layered feature of the exchange. However, it changes the thickness of the layers, being understood the thickness in terms of the salinity coordinate. The M4 contribution, which is known to account for the tidal asymmetry, increases the thickness of the upper outflowing layer at all cross-sections, except at $\mathrm{CS}_2$ and $\mathrm{CS}_5$ where the lower inflowing layer thickness increases. These changes are evidenced in the shift of the maxima of $Q(S)$ towards higher salinities and lower salinities, respectively. At all locations the maxima of the volume transports $Q(S)$ are about 10% larger when considering the superposition of M2 and M4 constituents.

Knudsen-consistent values (with and without the inclusion of M4) of volume transports, salinities, and salt transports obtained from $Q(S)$ and $q(S)$ in Fig. 6 are shown in Table 4. The largest differences due to the inclusion of the M4 are obtained in the cross-section closest to the mouth ($\mathrm{CS}_0$). At this cross-section, percentage differences in outgoing and incoming volume with and without the M4 contribution ($Q_{out}$ and $Q_{in}$) are $\sim 8\%$ and $\sim 9\%$, respectively, whereas differences in Knudsen-consistent salinities are smaller, viz. $\sim 5\%$ and $\sim 2\%$, respectively. This yields increases in outgoing and incoming salt transports ($Q^s_{out}$ and $Q^s_{in}$) $\sim 13\%$ and $\sim 11\%$, respectively. At other cross-sections differences in the Knudsen-bulk estimates for inflow and outflow of water and salt do not exceed $8\%$. These percentage values are not particularly large, but non-negligible either. This seems to ensue that the covariance between salinity and current is a mechanism more significant controlling the exchange flow in the Guadalquivir estuary than the tidal asymmetry. Notice that the ratio of the M4 and M2 amplitudes is below 16% for currents and below 13% for salinities, being the largest ratios observed at $\mathrm{CS}_0$ and $\mathrm{CS}_5$ (see Tables 2 and 3). These two locations are where differences in volume transport and exchange profiles shown in Fig. 6 are the largest.

### 3.3.2 Sensitivity Analysis

The effects on TEF due to the inclusion of the M4 in the tidal flow and salinity model depend on the relative differences of amplitudes and phases, thus they could differ in other estuaries or semi-enclosed basins. A sensitivity analysis of TEF to

https://doi.org/10.5194/egusphere-2025-6526
Preprint. Discussion started: 5 January 2026


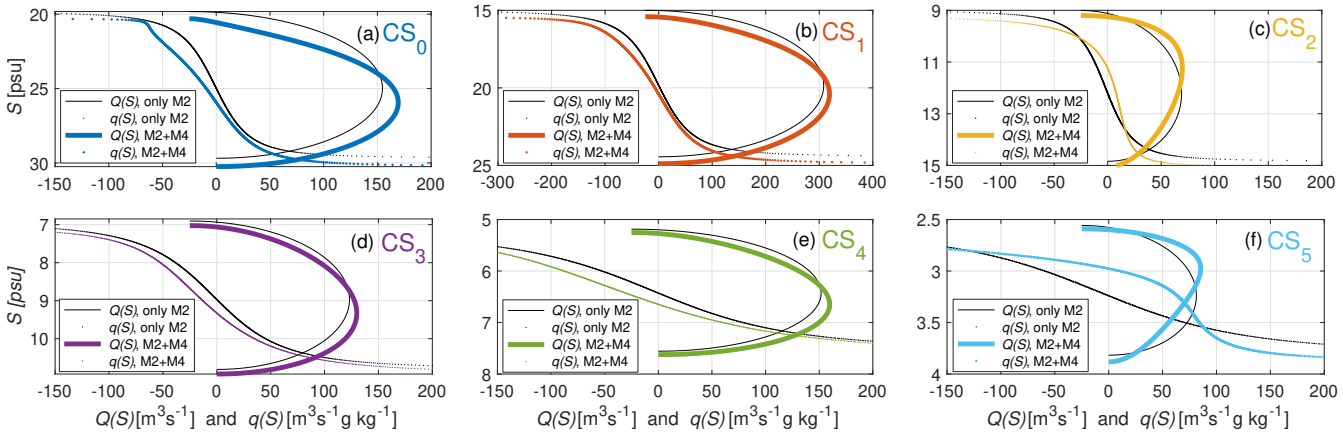


**Figure 6.** Volume transports $Q(S)$ (solid curves) and exchange profiles (dotted curves) $q(S)$ sorted by salinity classes are computed at cross-sections $\mathrm{CS}_i$ considering the superposition of the M2 and M4 constituents (colored curves) and the M2 only, without the M4 contribution (black curves).

**Table 4.** Knudsen-consistent outgoing and incoming volume transports ($Q_{out}$ and $Q_{in}$, respectively), salinities for out- and inflows ($s_{out}$ and $s_{in}$, respectively), and outgoing and incoming salt transports ($Q^s_{out}$ and $Q^s_{in}$, respectively) with and without the M4 contribution, i.e., with the M2 tide only, at each cross-section $\mathrm{CS}_i$.

| - | $\mathrm{CS}_0$ | $\mathrm{CS}_1$ | $\mathrm{CS}_2$ | $\mathrm{CS}_3$ | $\mathrm{CS}_4$ | $\mathrm{CS}_5$ | $\mathrm{CS}_6$ |
|---|---|---|---|---|---|---|---|
| $Q_{out}\,[\mathrm{m^3s^{-1}}]$ | -194.4 | -344.1 | -94.74 | -154.9 | -184.8 | -110.0 | -25 |
| $Q_{out}$, M2 only | -179.7 | -333.2 | -94 | -148.1 | -176.8 | -106.3 | -25 |
| $Q_{in}\,[\mathrm{m^3s^{-1}}]$ | 169.4 | 319.1 | 69.74 | 129.9 | 159.8 | 85.32 | 0 |
| $Q_{in}$, M2 only | 154.7 | 308.2 | 69 | 123.2 | 151.8 | 81.33 | 0 |
| $s_{out}\,[\mathrm{psu}]$ | 22.03 | 16.68 | 9.56 | 7.58 | 5.61 | 2.67 | 0 |
| $s_{out}$, M2 only | 20.94 | 16.04 | 9.70 | 7.35 | 5.45 | 2.70 | 0 |
| $s_{in}\,[\mathrm{psu}]$ | 29.3 | 23.9 | 14.02 | 10.6 | 7.42 | 3.59 | 0 |
| $s_{in}$, M2 only | 28.68 | 23.46 | 14.28 | 10.42 | 7.31 | 3.69 | 0 |
| $Q^s_{out}\,[\mathrm{m^3s^{-1}psu}]$ | -4283 | -5741 | -905.6 | -1174 | -1036 | -294.3 | 0 |
| $Q^s_{out}$, M2 only | -3762 | -5345 | -911.8 | -1089 | -964.3 | -287.6 | 0 |
| $Q^s_{in}\,[\mathrm{m^3s^{-1}psu}]$ | 4964 | 7626 | 978.1 | 1377 | 1186 | 306.2 | 0 |
| $Q^s_{in}$, M2 only | 4437 | 7231 | 985.4 | 1283 | 1111 | 300.4 | 0 |

values of current and salinity amplitudes and phases (i.e. those in Eqs. 8a and 8b) and freshwater discharge is thus performed considering values at $\mathrm{CS}_1$ in the Guadalquivir estuary as reference. The analysis is performed only during the low riverflow conditions for $R = 10\,\mathrm{m^3s^{-1}}$, $25\,\mathrm{m^3s^{-1}}$, and $40\,\mathrm{m^3s^{-1}}$. The analysis considers as reference parameters those observed in the cross-section $\mathrm{CS}_1$, which exhibits the largest exchange flow in the Guadalquivir estuary, viz. $A = 4135\,\mathrm{m^2}$, $u_a = 1\,\mathrm{ms^{-1}}$, $s_r = 19.72\,\mathrm{g\,kg^{-1}}$, $s_a = 4.72\,\mathrm{g\,kg^{-1}}$, and $\psi_b = 127.11°$. The residual current is $u_r = -0.0024\,\mathrm{ms^{-1}}$ for $R = 10\,\mathrm{m^3s^{-1}}$, $u_r =$

https://doi.org/10.5194/egusphere-2025-6526
Preprint. Discussion started: 5 January 2026


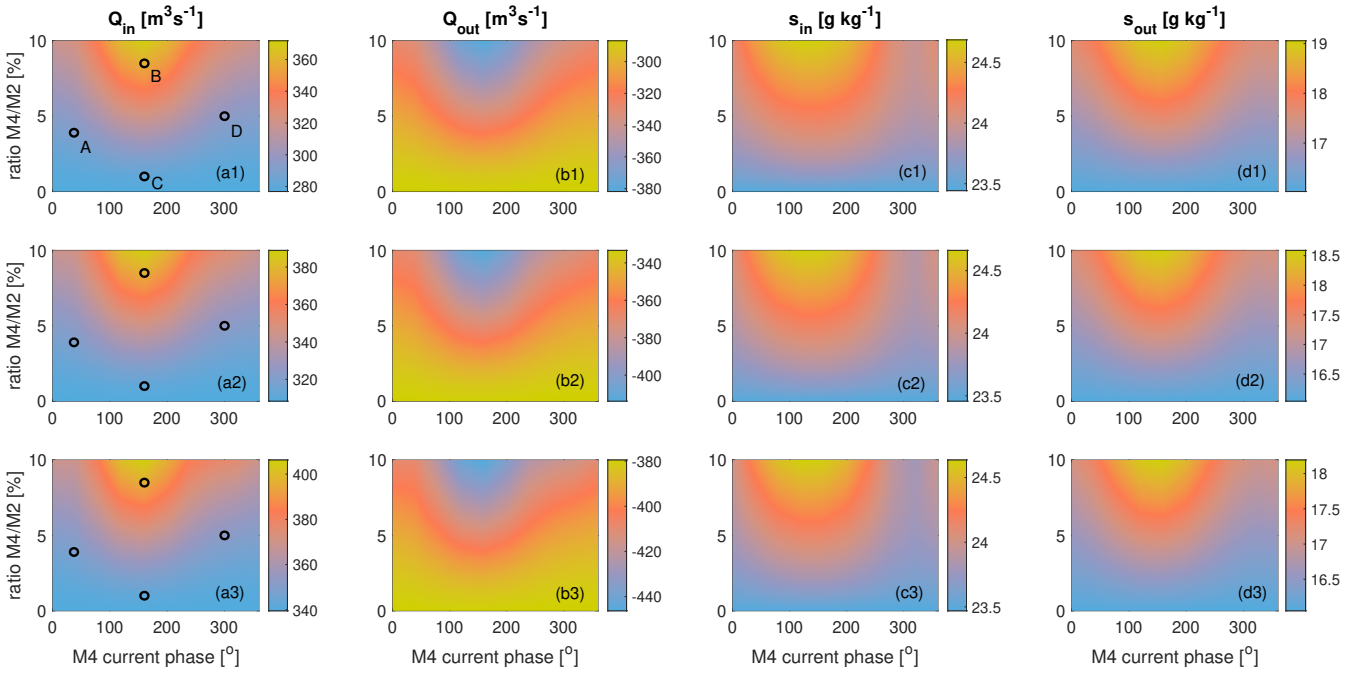


**Figure 7.** Sensitivity of Knudsen-consistent incoming (panels a1, a2, and a3) and outgoing volume transports (panels b1, b2, and b3) and salinities for inflows (panels c1, c2, and c3) and outflows (panels d1, d2, and d3) to ratio between M4 and M2 current amplitudes ($u_b/u_a$) and to M4 current phase ($\varphi_b$). First, second and third row of panels correspond with $R = 10\,\mathrm{m^3 s^{-1}}$, $R = 25\,\mathrm{m^3 s^{-1}}$, and $R = 40\,\mathrm{m^3 s^{-1}}$, respectively. Black circles and capital letters indicate example cases in the parameter space shown in Fig. 8.

$-0.0060\,\mathrm{m\,s^{-1}}$ for $R = 25\,\mathrm{m^3 s^{-1}}$, and $u_r = -0.0097\,\mathrm{m\,s^{-1}}$ for $R = 40\,\mathrm{m^3 s^{-1}}$. The M2 salinity phase $\psi_a$ is determined from the zero residual salinity flux condition (Eq. 10). The ratio between M4 and M2 current amplitudes, $u_b/u_a$, is varied from $0\%$ to $10\%$. The ratio between M4 and M2 salinity amplitudes, $s_b/s_a$, consistently varies along with the currents from $0$ to $0.9059$. Current and salinity M4 and M2 amplitudes are chosen not to be independent to match observations in $\mathrm{CS}_1$ when $u_b = 0.039\,\mathrm{m\,s^{-1}}$, $s_b = 0.4767\,\mathrm{g\,kg^{-1}}$ (Tables 2 and 3), and also when $u_b = 0$, $s_b = 0$ (which corresponds with the only M2 case). The difference between M4 current and salinity phases, $\varphi_b - \psi_b$, is varied from $0°$ and $360°$.

The inclusion of M4 term in the tidal model significantly influences Knudsen-consistent quantities of the exchange with regards to the M2 only reference case. The results of this analysis yield differences in volume transports, salinities, and salt transports. Figure 7 shows patterns of incoming ($Q_{in}$, panels a) and outgoing volume transports ($Q_{out}$, panels b) and their respective consistent salinities $s_{in}$ (panels c) and $s_{out}$ (panels d) in the explored parameter space for $R = 10\,\mathrm{m^3 s^{-1}}$ (upper row), $R = 25\,\mathrm{m^3 s^{-1}}$ (middle row), and $R = 40\,\mathrm{m^3 s^{-1}}$ (lower row). Values for the only M2 reference case correspond with the ratio of M4 and M2 current amplitude $u_b/u_a = 0$. Overall, for $R = 10\,\mathrm{m^3 s^{-1}}$ (upper panels in Fig. 7), the higher the ratio of M4 and M2 current amplitudes ($u_b/u_a$) and the closer to $\sim 160°$ the M4 current phase ($\varphi_b$) is, the higher the influence in $Q_{in}$ (panel a1), $Q_{out}$ (b1), $s_{in}$ (c1), and $s_{out}$ (d1). Differences in $Q_{in}$ and $Q_{out}$ between cases including M4 and the case with

https://doi.org/10.5194/egusphere-2025-6526
Preprint. Discussion started: 5 January 2026


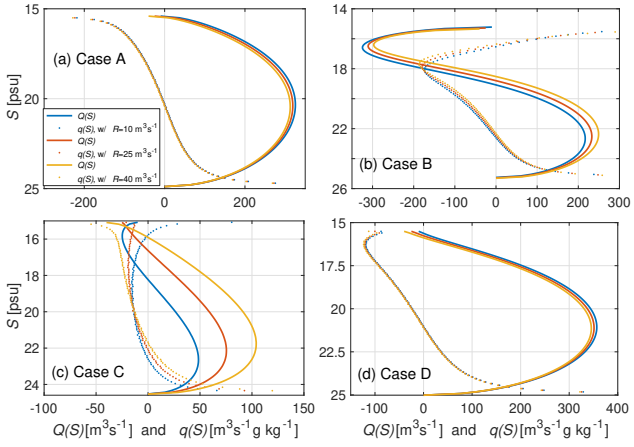


**Figure 8.** Volume transports $Q(S)$ (solid curves) and exchange profiles $q(S)$ (dotted curves) for cases A, B, C, and D marked with black circles in the parameter space in panels a1 ($R = 10\,\mathrm{m^3 s^{-1}}$), a2 ($R = 25\,\mathrm{m^3 s^{-1}}$), and a3 ($R = 40\,\mathrm{m^3 s^{-1}}$) of Figure 7. Legend is common to the four panels.

only M2 can be as much as $\pm 94\,\mathrm{m^3 s^{-1}}$ when the ratio of amplitudes is $u_b/u_a \approx 0.10$, thereby being $Q_{in} \approx 371\,\mathrm{m^3 s^{-1}}$ (panel a1) and $Q_{out} \approx -381\,\mathrm{m^3 s^{-1}}$ (panel b1). Salinity for inflows increases due to the inclusion of the M4 up to $s_{in} = 24.7\,\mathrm{psu}$ (+1.2 psu, panel c1), whereas for outflows increases up to $s_{out} = 19.0\,\mathrm{psu}$ (+3.0 psu, panel d1).

Patterns of the same variables for $R = 25\,\mathrm{m^3 s^{-1}}$ and $R = 40\,\mathrm{m^3 s^{-1}}$ are shown in the second and third rows of panels, respectively. The highest bulk values in $Q_{in}$ (panels a2 and a3, respectively), $Q_{out}$ (panels b2 and b3, respectively), $s_{in}$ (panels c2 and c3, respectively), and $s_{in}$ (panels d2 and d3, respectively) also occur for large M4 vs. M2 current amplitude ratios and M4 current phase values $\varphi_b \approx 160°$. Results also indicate that the higher the freshwater discharge, the higher the exchange. For $R = 25\,\mathrm{m^3 s^{-1}}$, the highest incoming volume transport bulk value is $Q_{in} \approx 388.90\,\mathrm{m^3 s^{-1}}$ (panel a2) and the lowest outgoing volume attained is $Q_{out} \approx -413.90\,\mathrm{m^3 s^{-1}}$ (panel b2). These values differ about $80\,\mathrm{m^3 s^{-1}}$ from what is observed in $\mathrm{CS_1}$ in the Guadalquivir estuary, i.e. for $R = 25\,\mathrm{m^3 s^{-1}}$, $Q_{in} = 308.2\,\mathrm{m^3 s^{-1}}$, $Q_{out} = -333.2\,\mathrm{m^3 s^{-1}}$ (same parameters as Case A, and also in Table 4). For $R = 40\,\mathrm{m^3 s^{-1}}$, the highest incoming and outgoing transports ($Q_{in} \approx 406.25\,\mathrm{m^3 s^{-1}}$ (panel a3) and $Q_{out} \approx -446.25\,\mathrm{m^3 s^{-1}}$) (panel b3) occur at the same phase.

Additionally, in the parameter space explored, as the freshwater discharge increases, both the $s_{in}$ and $s_{out}$ values tend to decrease. Regarding differences with respect to the only M2 case, the maxima/minima $s_{in}$ values slightly decrease/increase with increasing freshwater discharge, i.e. from $23.44 - 24.68\,\mathrm{psu}$ for $R = 10\,\mathrm{m^3 s^{-1}}$ (panel c1) to $23.46 - 24.63\,\mathrm{psu}$ for $R = 40\,\mathrm{m^3 s^{-1}}$ (panel c3). The maxima/minima $s_{out}$ values slightly decrease/increase with increasing freshwater discharge, i.e. from $16.02 - 19.05\,\mathrm{psu}$ for $R = 10\,\mathrm{m^3 s^{-1}}$ (panel c1) to $16.05 - 18.19\,\mathrm{psu}$ for $R = 40\,\mathrm{m^3 s^{-1}}$ (panel c3).

Figure 8 shows four example Cases (A, B, C, and D in panel a1 in Figure 7) of modified volume transports $Q(S)$ and exchange profiles $q(S)$ sorted by salinity classes which correspond with four sets of parameters for three different freshwater discharges (panels a1, a2, and a3). Overall, the inclusion of the M4 constituent changes thickness and magnitude of the bi-layer

https://doi.org/10.5194/egusphere-2025-6526
Preprint. Discussion started: 5 January 2026


exchange flow by salinity class. The extent of the change depends on the ratio between M4 and M2 current amplitudes ($u_b/u_a$) and to M4 current phase ($\varphi_b$). Case A (panel a in Fig. 8) represents the parameters observed at $\mathrm{CS}_1$, incorporating the M4 and M2 tidal constituents for various freshwater discharge rates. This case indicates that the inclusion of M4, relative to the M2-only scenario, increases the thickness of the upper layer of the $q(S)$ profile for all discharge values, viz. $R = 10\,\mathrm{m^3 s^{-1}}$ (blue curve), $R = 25\,\mathrm{m^3 s^{-1}}$ (red curve), and $R = 40\,\mathrm{m^3 s^{-1}}$ (yellow curve). This effect is more pronounced at higher river flows, though the differences are not substantial. Similar patterns are observed in Case D (panel d in Fig. 8), which displays $q(S)$ profiles for comparable M4 vs. M2 ratios to those of Case A but with $\varphi_b \approx 300°$. In Case D, it is likewise observed that the inclusion of M4 increases the thickness of the upper layer of the $q(S)$ profile compared to the M2-only for the three discharge values simulated, although, again, without significant variations. A slight intensification of the outflows is observed near the lowest salinity classes ($S_{min}$ in Eq. 3). In both Cases A and D, for a given salinity class, the volume transport $Q(S)$ decreases with decreasing discharge.

More significant changes occur for phases $\varphi_b \approx 160°$ for both low and high ratios between M4 and M2 current amplitudes. In Case B (panel b in Fig. 8), characterized by higher M4 vs. M4 amplitude ratios in both current and salinity, inflow (positive $q(S)$ values) is observed at low salinity classes. This is a consequence of the covariance between current and salinity, which governs the integrated salt flux. This phenomenon occurs for this Case B for the three simulated discharges $R = 10$, 20, and $40\,\mathrm{m^3 s^{-1}}$. In Case C, the M4 vs. M2 ratio is smaller, and the exchange transports per salinity class are lower. An increase in the thickness of the upper layer of the $q(S)$ profile relative to the M2-only case is evident for all three freshwater discharge values. In this case, inflow is only observed for $q(S)$ over a narrow range of low-salinity classes. Higher freshwater discharge shifts the $q(S)$ profile toward negative (outflowing) values.

## 4 Conclusions

A well-mixed $\mathrm{M2} + \mathrm{M4}$ tidal flow and salinity model is applied to the Guadalquivir estuary to estimate Total Exchange Flow (TEF) for the first time at notable cross-sections, including the mouth, during low river flow conditions. Estimates are determined combining the modeling approach with high-resolution field measurements of currents and salinity along the main channel. A sensitivity analysis of exchange profiles and volume transports to the inclusion of the M4 constituent to the tidal flow and salinity model. The results of this study translated into the following conclusions.

Knudsen-consistent along-channel TEF estimates decrease upstream in the Guadalquivir estuary. Incoming and outgoing water volume transports are about 10% larger than previous estimates based on gravitational circulation only. In the middle part of the estuary, incoming TEF bulk volume values below $150\,\mathrm{m^3 s^{-1}}$ are obtained. The largest net incoming water volume transport, viz. approx. $300\,\mathrm{m^3 s^{-1}}$, is attained at the lower part of the estuary, near where the largest salinity gradient is observed. This value is about 12-fold the normal river flow from the head dam at Alcalá del Río. Its corresponding representative TEF bulk salinity value is $20\,\mathrm{psu}$, whereas the representative value for outflows at the same location is about $16\,\mathrm{psu}$. This evidences the poorly-stratified character of the Guadalquivir estuary, with a mixing completeness larger than 67% at all cross-sections. As expected, negligible values are obtained in the upper part of the estuary near the head dam.

https://doi.org/10.5194/egusphere-2025-6526
Preprint. Discussion started: 5 January 2026


The covariance between salinity and current seems to play a more important role in exchange flow in the Guadalquivir estuary than the effects due to tidal asymmetry. The inclusion of the M4 tidal constituent with regards to the original analysis of the M2(-only) tidal flow produces noticeable effects in Knudsen-consistent salinity values, volume transports and exchange profiles. Knudsen-consistent salinity values increased up to $5\%$. At all locations in the estuary, the maxima of the volume transport $Q(S)$ are about 10% larger when considering the superposition of M2 and M4 constituents.

The inclusion of the M4 yield differences with regard to the only-M2 case in volume transports and exchange profiles, and thus in volume transports, salinities, and salt transports. These differences could be even more significant in other semi-enclosed basins with higher tidal asymmetry than that of the Guadalquivir estuary. The sensitivity analysis shows that the M4 constituent changes thickness and magnitude of the bi-layer exchange flow by salinity class. The larger deviations from the reference case with the M2 term only occur when the ratio between M4 and M2 current amplitudes is larger, and the M4 current phase is closer to $160°$. The modified exchange profiles show in that case a remarkable inflow at low salinity classes.

Overall, this study contributes to further understanding TEF in weakly-stratified estuaries. Estimates provided in this work, which are based on a simple tidal model and field data from a comprehensive field campaign, could serve as a basis and touchstone for further works with more complex computational models in the Guadalquivir estuary. The low computational cost of the $\mathrm{M2}+\mathrm{M4}$ tidal flow and salinity model makes it particularly suitable to be applied systematically (and simultaneously) in a large number of estuaries at a regional scale. This approach allows studying trends in TEF caused by climate-scale changes in freshwater discharges, salinity distribution, and tidal parameters in estuaries.

*Author contributions.* Conceptualization: M.D-M., H.B. Data Curation: M.D-M. Formal Analysis: M.D-M., H.B. Investigation: M.D-M., H.B. Methodology: M.D-M., H.B. Resources: M.D-M. Software: M.D-M. Supervision: M.D-M., H.B. Validation: M.D-M. Visualization: M.D-M. Writing – Original Draft: M.D-M. Writing – Review Editing: M.D-M., H.B.

*Competing interests.* The authors declare that they have no conflict of interest.

*Acknowledgements.* Authors acknowledge support from BARRIER project (Ministerio de Ciencia, Innovación y Universidades, PID2023-148298OA-I00), Working Group 172 “Oceanic Salt Intrusion into Tidal Freshwater Rivers" (SALTWATER) of the Scientific Committee on Oceanic Research (SCOR), and EPICOS project (Junta de Andalucía - Consejería de Universidad, Investigación e Innovación, Plan Andaluz de Investigación, Desarrollo e Innovación; Ref. ProyExcel_00375). Observational data of the Guadalquivir Estuary are available from https://doi.org/10.5281/zenodo.3459610 (CC BY 4.0 license).

https://doi.org/10.5194/egusphere-2025-6526
Preprint. Discussion started: 5 January 2026


## References

Biemond, B., de Swart, H. E., and Dijkstra, H. A.: Quantification of salt transports due to exchange flow and tidal flow in estuaries, Journal of Geophysical Research: Oceans, 129, e2024JC021 294, 2024.

Burchard, H.: A universal law of estuarine mixing, Journal of Physical Oceanography, 50, 81–93, 2020.

Burchard, H., Bolding, K., Feistel, R., Gräwe, U., Klingbeil, K., MacCready, P., Mohrholz, V., Umlauf, L., and van der Lee, E. M.: The Knudsen theorem and the Total Exchange Flow analysis framework applied to the Baltic Sea, Progress in oceanography, 165, 268–286, 2018a.

Burchard, H., Schuttelaars, H. M., and Ralston, D. K.: Sediment trapping in estuaries, Annual Review of Marine Science, 10, 371–395, 2018b.

Burchard, H., Lange, X., Klingbeil, K., and MacCready, P.: Mixing estimates for estuaries, Journal of Physical Oceanography, 49, 631–648, 2019.

Burchard, H., Klingbeil, K., Lange, X., Li, X., Lorenz, M., MacCready, P., and Reese, L.: The relation between exchange flow and diahaline mixing in estuaries, Journal of Physical Oceanography, accepted for publication, 2025.

Caballero, I., Morris, E. P., Ruiz, J., and Navarro, G.: Assessment of suspended solids in the Guadalquivir estuary using new DEIMOS-1 medium spatial resolution imagery, Remote Sensing of Environment, 146, 148–158, 2014.

Cobos, M., Baquerizo, A., Díez-Minguito, M., and Losada, M.: A subtidal box model based on the longitudinal anomaly of potential energy for narrow estuaries. An application to the Guadalquivir River Estuary (SW Spain), Journal of Geophysical Research: Oceans, 125, e2019JC015 242, 2020.

Cokelet, E. and Stewart, R.: The exchange of water in fjords: The efflux/reflux theory of advective reaches separated by mixing zones, Journal of Geophysical Research: Oceans, 90, 7287–7306, 1985.

de Swart, H. and Zimmerman, J.: Morphodynamics of tidal inlet systems, Annual review of fluid mechanics, 41, 203–229, 2009.

Díez-Minguito, M. and de Swart, H. E.: Relationships Between Chlorophyll-a and Suspended Sediment Concentration in a High-Nutrient Load Estuary: An Observational and Idealized Modeling Approach, Journal of Geophysical Research: Oceans, 125, e2019JC015 188, 2020.

Díez-Minguito, M., Baquerizo, A., Ortega-Sánchez, M., Navarro, G., and Losada, M. A.: Tide transformation in the Guadalquivir estuary (SW Spain) and process-based zonation, Journal of Geophysical Research: Oceans (1978–2012), 117(C3), 2012.

Díez-Minguito, M., Contreras, E., Polo, M. J., and Losada, M. A.: Spatio-temporal distribution, along-channel transport, and post-riverflood recovery of salinity in the Guadalquivir estuary (SW Spain), Journal of Geophysical Research: Oceans, 118, 2267–2278, 2013.

Díez-Minguito, M., Baquerizo, A., de Swart, H. E., and Losada, M. A.: Structure of the turbidity field in the Guadalquivir estuary: Analysis of observations and a box model approach, Journal of Geophysical Research: Oceans, 119, 7190–7204, 2014.

Friedrichs, C. T. and Aubrey, D. G.: Tidal propagation in strongly convergent channels, Journal of Geophysical Research: Oceans (1978–2012), 99, 3321–3336, 1994.

Knudsen, M.: Ein hydrographischer Lehrsatz, Ann. Hydrogr. Mar. Meterol., 28, 316–320, 1900.

Lorenz, M., Klingbeil, K., MacCready, P., and Burchard, H.: Numerical issues of the Total Exchange Flow (TEF) analysis framework for quantifying estuarine circulation, Ocean Science, 15, 601–614, 2019.

MacCready, P.: Calculating estuarine exchange flow using isohaline coordinates, Journal of Physical Oceanography, 41, 1116–1124, 2011.

https://doi.org/10.5194/egusphere-2025-6526
Preprint. Discussion started: 5 January 2026


MacCready, P., Geyer, W. R., and Burchard, H.: Estuarine exchange flow is related to mixing through the salinity variance budget, Journal of Physical Oceanography, 48, 1375–1384, 2018.

Muñoz-Lopez, P., Nadal, I., García-Lafuente, J., Sammartino, S., and Bejarano, A.: Numerical modeling of tidal propagation and frequency responses in the Guadalquivir estuary (SW, Iberian Peninsula), Continental Shelf Research, 279, 105 275, 2024.

Navarro, G., Gutierrez, F. J., Díez-Minguito, M., Losada, M. A., and Ruiz, J.: Temporal and spatial variability in the Guadalquivir Estuary: A challenge for real-time telemetry, Ocean Dynamics, 61, 753–765, 2011.

Parker, B. B.: The relative importance of the various nonlinear mechanisms in a wide range of tidal interactions, in Tidal hydrodynamics, pp. 237–268, 1991.

Pawlowicz, R., Beardsley, B., and Lentz, S.: Classical tidal harmonic analysis including error estimates in MATLAB using T_TIDE, Computers & Geosciences, 28, 929–937, 2002.

Reese, L., Gräwe, U., Klingbeil, K., Li, X., Lorenz, M., and Burchard, H.: Local mixing determines spatial structure of diahaline exchange flow in a mesotidal estuary: A study of extreme runoff conditions, Journal of Physical Oceanography, 54, 3–27, 2024.

Reyes-Merlo, M. Á., Díez-Minguito, M., Ortega-Sánchez, M., Baquerizo, A., and Losada, M. Á.: On the relative influence of climate forcing agents on the saline intrusion in a well-mixed estuary: Medium-term Monte Carlo predictions, Journal of Coastal Research, pp. 1200–1205, 2013.

Sirviente, S., Sánchez-Rodríguez, J., Gomiz-Pascual, J. J., Bolado-Penagos, M., Sierra, A., Ortega, T., Álvarez, O., Forja, J., and Bruno, M.: A numerical simulation study of the hydrodynamic effects caused by morphological changes in the Guadalquivir River Estuary, Science of The Total Environment, 902, 166 084, 2023.

Speer, P. and Aubrey, D.: A study of non-linear tidal propagation in shallow inlet/estuarine systems Part II: Theory, Estuarine, Coastal and Shelf Science, 21, 207–224, 1985.

Wang, T., Geyer, W. R., and MacCready, P.: Total exchange flow, entrainment, and diffusive salt flux in estuaries, Journal of Physical Oceanography, 47, 1205–1220, 2017.